A SOLAR REFLECTANCE METHOD FOR RETRIEVING CLOUD OPTICAL THICKNESS AND DROPLET SIZE OVER SNOW AND ICE SURFACES

S. Platnick[1,2], J. Y. Li[2,3], M. D. King[2], H. Gerber[4], P. V. Hobbs[5]

[1] University of Maryland Baltimore County, Baltimore, MD
[2] NASA Goddard Space Flight Center, Greenbelt, MD
[3] SM&AE Corporation, Vienna, VA, [4] Gerber Scientific Inc., Reston, VA
[5] University of Washington, Seattle, WA

Submitted to:
Journal of Geophysical Research – Atmospheres
FIRE-ACE Special Issue
15 December 1999

Corresponding author address:

S. Platnick
Code 913
NASA GSFC
Greenbelt, MD 20771
platnick@climate.gsfc.nasa.gov

Abstract

Cloud optical thickness and effective radius retrievals from solar reflectance measurements are traditionally implemented using a combination of spectral channels that are absorbing and non-absorbing for water particles. Reflectances in non-absorbing channels (e.g., 0.67, 0.86, 1.2 μm spectral window bands) are largely dependent on cloud optical thickness, while longer wavelength absorbing channels (1.6, 2.1, and 3.7 μm window bands) provide cloud particle size information. Cloud retrievals over ice and snow surfaces present serious difficulties. At the shorter wavelengths, ice is bright and highly variable, both characteristics acting to significantly increase cloud retrieval uncertainty. In contrast, reflectances at the longer wavelengths are relatively small and may be comparable to that of dark open water.

A modification to the traditional cloud retrieval technique is devised. The new algorithm uses only a combination of absorbing spectral channels for which the snow/ice albedo is relatively small. Using this approach, retrievals have been made with the MODIS Airborne Simulator (MAS) imager flown aboard the NASA ER-2 from May-June 1998 during the Arctic FIRE-ACE field deployment. Data from several coordinated ER-2 and University of Washington CV-580 *in situ* aircraft observations of liquid water stratus clouds are examined. MAS retrievals of optical thickness, droplet effective radius, and liquid water path are shown to be in good agreement with the in situ measurements. The initial success of the technique has implications for future operational satellite cloud retrieval algorithms in polar and wintertime regions.

1. Introduction

The First ISCCP (International Satellite Cloud Climatology Project) Regional Experiment – Arctic Clouds Experiment (FIRE-ACE) was conducted in the vicinity of Barrow, Alaska and northward over the Chukchi and Beaufort Seas. The overall purpose of the experiment was to better understand cloud-surface interactions and radiative effects in the Arctic Ocean region [see *Curry and al.*, 1999 for review]. Of specific interest to the FIRE project was development and validation of satellite and aircraft remote sensing techniques for retrieving cloud properties. In particular, retrievals of both cloud optical thickness and particle size are necessary in understanding and parameterizing cloud radiative effects in the shortwave and longwave spectral regions [*Slingo*, 1990; review of *Wielicki et al.*, 1995]. Cloud particle size retrievals are also important in studies of the so-called indirect effect of aerosols on climate, and in determining susceptibility to microphysical modification of cloud albedo [*Charlson et al.*, 1987; *Twomey*, 1974; *Twomey*, 1991] and precipitation processes [*Albrecht*, 1989; *Pincus and Baker*, 1994; *Austin et al.*, 1995]. In radiative studies, it is the *effective radius* ($r_e = \overline{r^3}/\overline{r^2}$) that is the important measure of the particle size distribution. Retrievals of both cloud parameters are especially problematic using solar reflectance techniques in the presence of highly reflective surfaces such as snow and sea ice in the polar regions. The FIRE-ACE time period overlapped with the Surface Heat Budget of the Arctic Ocean (SHEBA) project, which included an icebreaker ship adrift in the pack ice. The ice station, located about 700km northwest of Barrow, AK during the experiment, included a number of remote sensing and meteorological instruments useful in cloud retrieval validation.

Previous algorithms for retrieving cloud optical thickness and effective radius from reflectance measurements have used spectral bands that are both absorbing and non-absorbing for water particles. Reflectances in non-absorbing channels (e.g., 0.67, 0.86, 1.2μm spectral window bands) are largely dependent on cloud optical thickness. Only a relatively small decrease in reflectance occurs with increasing particle size due to a corresponding slight increase in the particle forward scattering (characterized by the scattering asymmetry parameter, g). For instance, the asymmetry parameter for liquid water droplets varies from only about 0.84 to 0.87 in the visible, as effective radius increases from 5 to 20μm. However, reflectances in longer wavelength absorbing channels (1.6, 2.1, and 3.7μm window bands, collectively referred to as *near-infrared* in

this paper) are extremely sensitive to particle absorption. Single scattering albedo (difference between unity and fractional particle absorption) decreases in the 2.1 μm band from about 0.99 to 0.96 for the same range of effective radii as in the above example. Since particle absorption is proportional to size, this sensitivity to single scattering albedo provides cloud particle size information. Such a combination of absorbing and non-absorbing reflectance measurements is advantageous in that it allows for a nearly orthogonal separation of optical thickness and particle size in the measurements, especially for thicker clouds (see section 2).

In principle, this technique is useful for ice particles as well as liquid water droplets. However, ice clouds will in general present an additional retrieval unknown – particle habit. Liquid water cloud retrievals, along with validation case studies, have been described by *Twomey and Cocks* [1982; 1989], *Foot* [1988], *Nakajima and King* [1990], *Nakajima et al.* [1991], and *Platnick and Valero* [1995]. Ice cloud retrieval validation studies [e.g., *Ou et al.*, 1995; *Young et al.*, 1998] have also been discussed. In the present study, we will deal *exclusively* with liquid water cloud retrievals using solar reflectance measurements. Since section 2 of this paper will only discuss basic retrieval principles, the reader is referred to the cited studies for further detail.

The use of a visible or other useful non-absorbing bands presents serious difficulties for cloud retrievals over ice and snow surfaces. At these shorter solar wavelengths, snow/ice can be both bright and highly variable, each acting to significantly increase cloud retrieval uncertainty. Retrieval algorithms are inherently more sensitive over dark surfaces where the cloud-surface contrast is greatest. Bright surfaces (e.g., an ice albedo of 0.5 in the visible) acts to reduce, or mask, the effect of the cloud on the overall measured reflectance. This is especially problematic for thin clouds having a reflectance of the same order as the surface reflectance variability. Of course, accurate knowledge of the surface reflectance is essential regardless of cloud thickness. In contrast, snow/ice reflectances at the longer wavelengths are relatively small and may be comparable to that of dark open water.

A modification to the traditional cloud retrieval technique is presented. The new algorithm uses only a combination of absorbing spectral channels for which the snow/ice albedo is relatively small. Specifically, the 1.6 μm band reflectance is essentially used as a surrogate for the traditional non-absorbing band, in conjunction with a more absorbing 2.1 or 3.7 μm band. This approach significantly reduces (or practically eliminates in the case studies that follow) the effect of the snow/ice surface. As nothing comes for free, the

reduced surface effect is at the expense of retrieval orthogonality. Using this method, liquid water cloud retrievals have been made with the MODIS Airborne Simulator (MAS) imager flown aboard NASA's high altitude ER-2 aircraft during the FIRE-ACE field deployment. While the FIRE-ACE observation period extended from April to July 1998, ER-2 operations were conducted between 18 May and 6 June out of Fairbanks, AK.

The MAS is a 50 channel scanning radiometer providing spectral coverage from the visible through the infrared, including those bands useful for cloud retrieval studies, via four separate grating assemblies. Onboard blackbodies are used for thermal calibration, while a laboratory integrating sphere is used in the solar spectrum. Spectral laboratory calibrations are also routinely made. At nominal ER-2 altitudes (20km), the nadir spatial resolution is 50m at the surface corresponding to a cross-track swath width of about 37km (716 pixels). Further details are given by *King et al.* [1996]. Cloud retrieval validation studies using this instrument have been reported by *Platnick et al.* [2000] for California marine stratus clouds.

In this paper, data from coordinated ER-2 and University of Washington CV-580 aircraft observations of liquid water stratus clouds are examined. Size retrievals are compared with *in situ* cloud profile measurements of effective radius made with the Particle Measuring Systems FSSP-100 probe. Optical thickness and liquid water path retrievals are compared with values derived from the Gerber Scientific, Inc. cloud integrating nephelometer (also known as the "*g*-meter") and PVM-100A [*Gerber et al.*, 1994], respectively. Section 2 discusses the difficulties of retrievals over bright surfaces and the tradeoffs in using only those spectral bands with significant water absorption. Section 3 summarizes sea ice and snow reflectance measurement in the Arctic obtained during previous field campaigns. In section 4 we discuss two liquid water cloud case studies, including a lowlevel boundary layer cloud and an extensive, but spatially variable, supercooled midlevel stratus deck. MAS retrievals are shown to be in good agreement with the *in situ* measurements.

2. Cloud Retrievals over Bright Surfaces

As discussed above, solar reflectance measurements in visible and near-infrared bands have been routinely used to infer cloud optical thickness (τ_c) and effective radius (r_e) of liquid water clouds. The reflectance in a visible or non-absorbing band has the

functional dependence $R_{VIS} \approx R_{VIS}(\tau_c)$, implying that optical thickness can largely be determined from this single measurement. In the water-absorbing near-infrared bands, located in the 1.6, 2.1, or 3.7 μm spectral region, reflectance can be a significant function of both quantities, i.e., $R_{NIR}=R_{NIR}(\tau_c,r_e)$, though for large absorption and/or cloud optical thickness, $R_{NIR} \approx R_{NIR}(r_e)$. Since these bands are located in atmospheric windows to minimize the effect of molecular absorption, further mention of absorption will be understood to refer to water droplets and not water vapor or other gases. Droplet size information can only be inferred from these absorbing bands. In principle, simultaneous reflectance measurements using a combination of any two bands (providing *at least* one has significant absorption) will allow for the solution of the two unknowns. For example, a combination of a 1.6 and 2.1 μm band reflectance measurement could be used instead of the traditional non-absorbing and absorbing band combination. However, only the latter combination allows for near othogonality between the two solutions. These concepts are discussed below.

Consider a cloud retrieval obtained from simultaneous visible and 2.1 μm band reflectance measurements for the ideal situation where the cloud overlies a surface having a small albedo in both bands. A useful means for understanding the information content of the two reflectance measurements is to transform the retrieval solution space (contours of constant optical thickness and effective radius) into the reflectance space [*Nakajima and King*, 1990; *Rawlins and Foot*, 1990]. An example is shown in the plots of Fig. 1a for the two corresponding MAS bands and the geometry given in the caption. The surface albedo for each, representative of open water, is indicated on the figure. With such a plot, the cloud retrieval problem reduces to the solution consistent with the point specified by reflectance measurement in the two spectral bands. Note that solution contours are nearly orthogonal over much of the measurement space, especially at the larger optical thicknesses. For exact orthogonality, an error in the reflectance measurement from one spectral band (caused by either instrument calibration or modeling errors) does not affect the solution obtained with the other spectral band. Though multiple solutions are seen for the 2 μm effective radius contour, such a size has been found to be unrealistic for real-world clouds.

Now consider a cloud overlying sea ice or snow. Figure 1b demonstrates the difficulties in retrieving cloud optical thickness using a spectral band for which the surface is both bright and variable. The retrieval solution space is shown for the same spectral bands of Fig. 1a, but with a Lambertian surface reflectance of 0.50 in the visible band. The surface albedo in the 2.1 μm band is assumed unchanged for an ice surface (see

section 3). Two sources for increased error sensitivity in the optical thickness contours are evident. First, the optical thickness contours have been moved to the right along the abscissa, narrowing their spacing. Because of this compression in the optical thickness contours, an error in the visible reflectance measurement will translates into a much greater optical thickness error than for the situation of Fig. 1a. This error magnification is inherent to retrievals over bright surfaces. The physical cause is the relatively smaller reflectance increase contributed by the cloud (even a semi-infinite cloud would not be detected with a non-absorbing band in the extreme case of unity surface albedo). Secondly, an uncertainty in the underlying sea ice albedo for the visible band results in an uncertainty in the horizontal position of the left side thickness contours (i.e., reflectance for ice plus thin cloud is highly uncertain) causing a potentially large retrieval uncertainty. As an example, inspection of Figs. 1a,b suggest that retrieval of optical thickness to within ±20% for a nominal cloud with τ_c=10 and r_e=10μm, would require knowing the surface reflectance to better than about 10% relative (i.e., 0.50±0.05). As discussed in the next section, sea ice and snow albedo can be highly variable with a significant seasonal variability. It is unrealistic to expect that the spectral surface albedo of these surfaces can be known to the desired accuracy, both temporally and spatially, for useful operational satellite cloud retrievals [*Wielicki et al.*, 1995]. Existence of broken sea ice, common near Barrow during FIRE-ACE, exacerbates the difficulty in specifying the effective area-averaged surface albedo needed for cloud retrievals.

A better quantitative approximation for the increased error sensitivity in the optical thickness retrieval from both these effects can be found from two-stream formulae for flux reflectance with conservative scattering. The combined cloud-surface reflectance is given by $R_m=R_c+R_s(1-R_c)^2/(1-R_sR_c)$ where R_m is the total *measured* reflectance, R_s is the surface reflectance, and R_c is the reflectance of the cloud being observed when overlying a black surface. Isolating the cloud reflectance terms gives $R_c=(R_m-R_s)/[1-R_s(2-R_m)]$. Substitution of a two-stream reflectance formula having the general form $R_c=\gamma\tau_c/(1+\gamma\tau_c)$, where τ_c is the cloud optical thickness and γ is a constant depending on the scattering asymmetry parameter, gives

$$\tau_c = \frac{1}{\gamma}\,\frac{R_m - R_s}{(1-R_m)(1-R_s)}\,. \qquad (1)$$

The above formula is a simple approximation for the *retrieved* optical thickness corresponding to some measured reflectance and a presumed surface reflectance. The small effect of droplet size on the retrieval (non-vertical contour lines in Fig. 1b) is through the asymmetry parameter, i.e., γ, which will be neglected in the following discussion.

Assuming the surface reflectance is specified without error, the relative uncertainty in the optical thickness retrieval due to measurement uncertainty (e.g., instrument calibration) is given by derivative $\partial \ln \tau_c / \partial R_m$. This corresponds to the first source of retrieval sensitivity discussed earlier. Retrieval uncertainty due to uncertainty in model calculations of the visible band reflectance is also covered by this derivative. It can be shown that the derivative is given by

$$\frac{\partial \ln \tau_c}{\partial R_m} = \frac{1}{\gamma \tau_c} \frac{1}{(1-R_m)^2} . \tag{2}$$

Likewise, because of symmetry between R_m and R_s in Eq. 1, the sensitivity to uncertainty in knowledge of the surface reflectance, assuming no measurement error, is

$$\frac{\partial \ln \tau_c}{\partial R_s} = \frac{-1}{\gamma \tau_c} \frac{1}{(1-R_s)^2} . \tag{3}$$

As an example, consider a cloud with τ_c=10, asymmetry parameter g=0.85, γ=(1-g)/2 [*Bohren*, 1987], and a surface reflectance of R_s=0.50, giving a cloud reflectance of R_c=0.43 and a total measured reflectance of R_m=0.64 (similar to FIRE-ACE cloud retrievals discussed in section 4). Then Eq. 3 implies that an increase in R_s of 0.05 would result in a decrease in the retrieved cloud optical thickness by over 25%. Or alternatively, if the retrieval is made with an assumption that R_s=0.50, but the actual value is R_s=0.55, then the relative error in the retrieved optical thickness is $\Delta\tau_c/\tau_c \approx +30\%$. Similarly, Eq. 2 gives a retrieval error of $\Delta\tau_c/\tau_c \approx +50\%$ if the measured reflectance R_m is in error by an amount of +0.05. In contrast, for the identical cloud over a dark surface with the assumption R_s=0.05, resulting errors due to the same underestimation in the surface reflectance and overestimation in the measured reflectance are reduced to $\Delta\tau_c/\tau_c \approx +7\%$

and +22%, respectively. In summary, for this rather typical cloud, optical thickness retrieval uncertainty due to a realistic uncertainty in the knowledge of the underlying sea ice surface reflectance, is greater by about a *factor of four* than retrieval uncertainty caused by a similar absolute uncertainty in the reflectance of a dark surface. Retrieval uncertainty due to measurement error is increased by a factor of two when the ice surface is present.

As discussed, the use of a non-absorbing band is not inherent to the retrievals, and two absorbing bands can also be used. The snow/ice surface albedo can be very small in all near-infrared bands as shown in the next section. Accordingly, Fig. 2a shows the solution space when the visible channel is replaced by a 1.6μm channel (absorbing for cloud droplets but much less than for the 2.1μm band). Again, a surface albedo equivalent to that of open water was used in generating the plots. While a simple analytic approximation is no longer feasible for this situation because of droplet absorption, such a retrieval would clearly have little dependence on sea ice characteristics, or fractional ice coverage. The disadvantage is that the solutions no longer have an orthogonal region, and so measurement error in one channel will *always* cause error in the retrieval of both cloud parameters. Specifically, retrieval error in one parameter causes a proportional (same sign) error in the other. An increased sensitivity to measurement error, when compared to the traditional non-absorbing band method with a dark surface, is also evident. Figure 2b shows the improved situation obtained with use of a 3.7μm band. However, cloud thermal emission in this band (also dependent on optical thickness and effective radius) can be a significant part of the measured upwelling radiance, thereby complicating the retrieval [*Arking and Childs*, 1985; *Han et al.*, 1994; *Platnick and Twomey*, 1994].

3. Spectral Albedo Measurements of Arctic Sea Ice and Snow

The utility of near-infrared water absorbing bands for cloud retrievals over snow/ice surfaces requires a small, hopefully insignificant, albedo in this spectral region compared with shorter wavelengths. Ground-based snow/ice spectral surface albedo and bidirectional reflectance measurements have been reported for a variety of locations and seasons. However, our particular interest is in large area-averaged measurements of albedo in those particular visible and near-infrared spectral bands useful for cloud retrievals. Such data is available from the Cloud Absorption Radiometer (CAR) flown aboard a low-flying aircraft during previous Arctic field campaigns.

The CAR is a narrowband visible/near-infrared scanning radiometer mounted in the nose cone of the University of Washington Convair CV-580 aircraft (previously on the University of Washington C-131A). Spectral channels include the 0.68, 0.87, 1.2, 1.6, and 2.1 μm bands. Though originally designed for use in thick cloud layers, the instrument's unique 190° zenith-to-nadir scanning capability also allows it to be used to map surface hemispheric upwelling bidirectional radiance fields. Such measurements are obtained as the aircraft flies repeated circles (approximately 3km in diameter) over a study site, at a typical altitude of 0.5-1.0km. Aircraft roll during the circular flight tracks is compensated for by rotating the CAR assembly within the nose cone. Surface albedo is derived from integration over the CAR upward hemispheric radiance measurements in conjunction with solar spectral flux tables. The derived albedo is effectively averaged over a spatial scale on the order of 3km (95% of the reflected energy is captured within this scale for isotropic reflectance). Further details of the instrument and algorithm are given in *Tsay et al.* [1988] and *Arnold et al.* [2000].

CAR bidirectional measurements were made during two previous Arctic field deployments: the Arctic Lead Experiment (LEADEX) during April 1992 and the June 1995 Arctic Radiation Measurements in Column Atmosphere-Surface System (ARMCAS). As with the FIRE-ACE campaign, both experiments were conducted in the vicinity of Barrow, AK and north over the Beaufort and Chukchi seas. A complete analysis of the reflectance data, including melt season sea ice, snow/ice over the tundra, and clear tundra is discussed by *Arnold et al.* [2000]. While such measurements can be made under diffuse conditions when higher cloud bases are present (more appropriate to the cloud retrieval problem), the analyzed data from these experiments was taken under clear sky conditions. Solar zenith angles in this region varied from about 65° to 50° between April and June during CAR acquisition times. A summary of the CAR albedo calculations for sea ice and snow/ice over tundra are given in Fig. 3. Albedo for the shorter wavelengths is seen to be large and variable, both being problematic for cloud retrievals (Fig. 1a; Eqs. 2, 3). In contrast, albedo in the 1.6 and 2.1 μm bands during June is only a few percent, similar to open water, and with relatively small variability. However, 1.6 μm snow/ice albedos in April are significantly larger than in June, though still much smaller than at shorter wavelengths (2.1 μm data not available). Figure 3 albedo calculations do not include an atmospheric correction appropriate to the aircraft altitude. However, it is exactly this combined surface-atmosphere albedo near cloud base that is relevant to the cloud retrieval problem.

The observed decrease in spectral sea ice albedo between April and June for the two previous field campaigns, were also found in solar broadband albedo aircraft measurements during FIRE-ACE [*Curry and al.*, 1999]. The CAR observations are also consistent with Arctic springtime ground observations of sea ice albedo under diffuse sky conditions [*DeAbreu et al.*, 1995; *Grenfell and Perovich*, 1984] where reflectance is reduced across the solar spectrum as overlying snow begins to melt. MAS bidirectional reflectance measurements of sea ice throughout the Barrow region during a clear sky ER-2 flight (29 May 1998) are also shown in Fig. 3. These data points also confirm the extremely low reflectance for the near-infrared bands during this time of year. So at least during the late springtime period, near-infrared ice/snow albedo in this region is likely to be comparable to dark open water and therefore ideally suited for cloud retrievals.

4. Liquid Water Cloud Retrievals from FIRE-ACE

Simultaneous cloud microphysical and optical thickness retrievals were performed on a variety of liquid water clouds imaged by the MAS during the FIRE-ACE ER-2 deployment period. Retrievals used the spectral technique described in section 2, with the 1.6μm band used as a surrogate for a non-absorbing band in conjunction with a 2.1 or 3.7μm band (e.g., Figs. 2a,b, respectively). Otherwise, the algorithm is identical to *Platnick et al.* [2000]. Of the 11 ER-2 flights flown from 18 May–6 June, coordinated cloud *in situ* sampling by the University of Washington CV-580 aircraft occurred during 6 of the flights. Two of these coordinations were in relatively uniform cloud regions useful for liquid water validation purposes. These case studies are discussed next.

4.1 Lowlevel boundary layer stratus cloud on 6 June 1998

An extensive boundary layer stratus cloud was overlying the coastal region along Barrow, AK at midday on 6 June 1998. The cloud was about 300m thick with a cloud-top height and temperature of about 800m and 268K, respectively. The ER-2 takeoff from Fairbanks, AK was at 1855UTC, with an objective to fly several flight legs over the Barrow region during the course of the day's flight. The CV-580 takeoff from Barrow was at 1941UTC, followed by *in situ* profile measurements during the subsequent ascent through the cloud layer. A second profile was made in this region at 2310UTC. Such vertical transits through the cloud are required for determining integrated optical and liquid water paths. Also, an appropriate weighting can then be applied to the effective

radius profile for comparison with the vertically-averaged reflectance-based retrievals [*Platnick*, 1999]. The coordination closest in time with the University of Washington CV-580 *in situ* measurements occurred during the initial ER-2 overpass at 2002UTC on the original northwest flight track out of Fairbanks. While this was 21 minutes after the first *in situ* profile, the later CV-580 profile showed just a small change in droplet effective radius over the three-and-one-half hour gap (cloud-top sizes increasing by about 1.3μm). Further, the retrievals discussed later indicate relatively uniform effective radii throughout the region at the time of the first ER-2 overpass.

Overflights of the North Slope of Alaska Atmospheric Radiation Measurement (NSA ARM) surface site near Barrow typically occurred several times during each ER-2 flight, including the initial flight from Fairbanks, AK out over the sea ice. This first pass over the ARM site generally occurred about the same time each day. As such, clear-sky MAS images of this region which were obtained twice in the week prior to the occurrence of the 6 June boundary layer cloud. These earlier images demonstrate the variable and often unpredictable nature of the land and ocean surface reflectances near the coast during this time of year. Figure 4a shows a geolocated visible MAS image over the Barrow area on 29 May 1998. Sea ice is seen to be widespread across the northern end of the image, with open water near the coast and snow/ice covering the tundra. Just four days later (Fig. 4b), the tundra has completely cleared of snow, though the myriad of melt-ponds remain frozen. Ice in the inlet southeast of Pt. Barrow has melted as well. Also, the offshore open water area appears to have diminished somewhat, with substantial sea ice fraction towards the southwest. Clearly, knowledge of such fine scale detail in the surface characteristics on a day-to-day basis would be extremely challenging for useful cloud validation studies, much less global scale retrievals. At the time of the MAS cloud observations three days later, the coastal open water area appeared to have diminished further as noted in CAR measurements made beneath the stratus cloud as the CV-580 was flying parallel to, and just offshore from the coast. MAS bidirectional reflectance measurements of the wet, recently melted, tundra obtained from the 2 June image (Fig. 4b) were found to be about 0.30±0.14, 0.06±0.04, and 0.04±0.03 in the 0.67, 1.6, and 2.1μm bands, respectively. Observations were for a solar zenith angle of 54° and with near-nadir views. No atmospheric corrections were made, a situation more applicable to the cloud retrieval problem which requires reflectance referenced to the cloud-base altitude. The low near-infrared surface reflectances, similar to that of the ice and open water, suggest that little discontinuity should be seen across the ocean-land boundary in the retrievals.

Figure 5a shows the visible MAS image at the time of the cloud retrieval on 6 June. The land-sea boundary is easily observed through the cloud. Frozen ponds are noted as well as the open water inlet southeast of Pt. Barrow. Conversely, because of the low albedo for all surfaces, the corresponding 1.6μm band image (Fig. 5b) shows a uniform cloud across the coastal area. A sharp boundary between a substantially thinner cloud region is seen towards the northeast of the image. This boundary is now observed to be a real feature of the cloud field and not an artifact of the underlying sea ice boundary. An atmospheric correction was applied to the MAS spectral measurements using an above-cloud column water vapor amount of $0.95\,\mathrm{g\,cm^{-2}}$ (estimated from a SHEBA ice station rawinsonde launched at 2300 UTC). Resulting optical thickness and effective radius retrievals using the 1.6 and 2.1 μm bands are shown in Figs. 6a,b. As expected, optical thickness retrievals do not show the underlying discontinuities observed in the visible band surface reflectance. In addition, effective radius retrievals are seen to be quite uniform throughout the area, ranging from just 8-10μm throughout much of the offshore cloud region. Liquid water path retrievals (approximated as $LWP \approx 0.67 \tau r_e$, in units of $\mathrm{g\,m^{-2}}$ with effective radius in micrometers) are shown in Fig. 6c. Though only exact for a vertically uniform cloud where differences between various relevant moments of the droplet size distribution can be ignored, the water path approximation is likely to be quite accurate (better than 10%) for similarly thick adiabatic clouds [*Platnick*, 1999]. Liquid water path results closely resemble the pattern of the optical thickness retrievals due to the narrow dispersion in droplet sizes.

MAS retrieval statistics from the validation region (comprised of over 6,500 pixels) are given in Table 1b. The table also gives *in situ* profile measurements of the vertically integrated liquid water path and optical thickness (derived from Gerber Scientific's PVM-100A and integrating nephelometer, respectively). Calibration coefficients for the PVM are traceable to standard methods [*Gerber et al.*, 1994] and recent glass bead tests. Nephelometer extinction measurements, at a visible wavelength, have an estimated uncertainty of 5-10%. The *in situ* effective radius given in the table is a vertical weighting of the FSSP-100 measurements, assuming an adiabatic profile [*Platnick*, 1999]. FSSP effective radius measurements were found to be in excellent agreement with PVM-derived calculations. There is a 20% overestimate in retrieved optical thickness relative to the *in situ* value, though effective radii agree to within a few percent. Liquid water path values are in found to be in excellent agreement, though it is seen that a water path estimate (see above formula) using the *in situ* optical thickness and effective radius is 13% lower than the integrated PVM measurements. This lack of

consistency might be due, in part, to the use of an independent measurement source for each parameter, coupled with small-scale microphysical variability. For instance, measured effective radii at the same cloud level often vary by one to two micrometers on this day. Validation conclusions are also made difficult by the small *in situ* sample region (consisting of a single profile), compared with area-averaged reflectance retrievals (where reflected photons sample a horizontal region on the order of several hundred meters for the cloud in question). Given these caveats, the results of Table 1b are very encouraging.

When retrievals from the validation region were performed using the 1.6 and 3.7 μm MAS band combination, average effective radii were 14.0μm (4-5μm larger than when using the 2.1μm band). Though some size discrepancy is expected since the average penetration depth varies with band droplet absorption, this large difference cannot be explained by the observed droplet size profile. Due to the lack of orthogonality seen in Fig. 2b, optical thickness retrievals were also larger by a similar fraction (average value of 15.3).

4.2 Midlevel stratus deck on 3 June 1998

A supercooled, midlevel stratus cloud (cloud-top temperature and height of 256K and 3.3km) covered the SHEBA ice station region on 3 June 1998. *In situ* profile measurements through the 600m thick cloud layer were obtained just northeast of the ice station at 2122UTC. Integrating nephelometer analysis of the volume-averaged particle asymmetry parameter in the visible is consistent with the existence of spherical (liquid) cloud particles. Though several modes of ice crystals were observed by the University of Washington PMS 2D-C probe (maximum dimensions of about 200μm and 2mm), concentrations were very small, about 0.15 per liter, suggesting that the cloud layer was almost entirely liquid water. Lidar data from the SHEBA site also indicates liquid water droplets at the overpass times (*T. Uttal and B. Orr*, personal communication). Measurement statistics are summarized in Table 1a. The upper range given for optical thickness accounts for the presence of a lower, separate cloud layer, observed between an altitude of 0.5-1km during the CV-580 profile. This lower layer is found to contribute an additional optical path of only 3, compared with about 11 for the midlevel cloud layer. Over the SHEBA site, radar and lidar data indicate the dissipation of a thin lower layer at about 2200UTC. However, the large-scale persistence of this optically thin layer throughout the validation region is not certain. Regardless, the potential ice particle

contribution to optical extinction from either layer is likely to be insignificant, and so a liquid water retrieval algorithm should be suitable for the combined layers, if present.

The ER-2 flew over the same cloud region at 2103UTC (about 20 minutes before the CV-580 sampling). A visible MAS image of this region is shown in the left panel of Fig. 7a (not geolocated); the imaged area is approximately 37km in the east-west dimension by 31km. The *in situ* measurements are well north of the distinct east-west cloud band whose northern boundary is seen just to the south of the ice station (note the eddies seen throughout the northern boundary region, apparently caused by horizontal shear-induced turbulence). A subsequent ER-2 overpass towards the southeast was made over the ice station about 30 minutes later (10 minutes after the *in situ* in situ profile) allowing two flight tracks to be included in the validation. The second pass showed the cloud band to be advecting to the north-northwest at about 4.5m/sec. The shape of the northern edge of the boundary was preserved during this time. It will be shown (Fig. 7a) that retrieval differences across this boundary can be significant, especially for effective radius. Variability within each cloud region is also substantial. It is therefore important to co-locate the cloud region corresponding to the CV-580 measurements with MAS imagery from the two ER-2 overpasses at earlier and later times. Assuming that all cloud parcels move with the same mean flow as the boundary, a simple estimate can be made for the forward and backward trajectory of the sampled cloud. In this manner, optical thickness and effective radius retrievals were averaged from the two flight tracks (an unweighted average of over 17,000 pixels from the first overpass image, and 4,000 pixels from the second overpass). An atmospheric correction was based on an above-cloud column water vapor amount of 0.3 gcm^{-2} (derived from a SHEBA rawinsonde launched from the ice station at 2300 UTC). Results, shown in Table 1a for the 1.6 and 2.1 μm band retrievals, are again in good agreement with the *in situ* measurements. The second number in the CV-580 column includes the contribution of the thin lower cloud layer. In contrast to the results of section 4.1, the *in situ* estimate of liquid water path based on optical thickness and effective radius agrees well with the retrievals, but is in excess of the integrated liquid water content measurement. The large-scale retrievals are shown in Fig. 7a. Liquid water path (not shown) ranges from about 30 gm^{-2} in the southern region as well as just to the north of the cloud band in the western edge of the image, to a maximum of about 110 gm^{-2} in the eastern eddies just inside the cloud band.

For comparison, retrievals made with the 1.6 and 3.7μm bands are shown in Fig. 7b. Effective radius retrievals are larger by about 3μm (an average of 11.2μm), with

an optical thickness increase of 55% (average of 22.7). The cause of this large effective radius discrepancy for both clouds is unknown. MAS retrievals of summertime California marine stratocumulus clouds have also shown significantly larger effective radii when using the 3.7μm and non-absorbing band combination [*Platnick et al.*, 2000]. In fact, absolute size retrieval differences are generally the same, about 4-5μm. As already mentioned, measured droplet size profiles do not account for the difference. For comparison, a retrieval case study for marine stratocumulus using the Advanced Very High Resolution Radiometer (AVHRR) 3.7μm channel on the NOAA polar orbiting satellites yielded better droplet size agreement [*Platnick and Valero*, 1995]. MAS radiometric measurements in the 3.7μm band would have to be increased by about 20% to give retrievals consistent with *in situ* profile measurements and 2.1μm band retrievals. Though instrument calibration is always a potential issue, emissivity analysis of the onboard blackbodies used in processing the 3.7μm band data is not thought to be a source for such an error. Increasing the amount of above-cloud water vapor absorption acts to reduce retrieved radii. However, for the 3 June case study, an increase in the column amount by over a factor of 9 (reduction in the 3.7μm band above-cloud nadir transmittance from 0.95 to 0.83) would be required to move retrievals into the *in situ* range. It should be noted that top-of-the-atmosphere solar spectral fluxes used in computing cloud reflectance for this band are in need of modern corroboration. A common source of data is from the compilation of *Thekaekara* [1974] which reports fluxes at 100nm intervals through this band. The 3.7μm band retrieval issue is clearly in need of further study.

5. Discussion and conclusions

An algorithm for retrieving cloud optical thickness and effective radius over ice and snow surfaces has been developed. Retrievals have been applied to imagery data obtained from the MODIS Airborne Simulator (MAS) instrument flown aboard the NASA ER-2 during the Arctic FIRE-ACE field deployment from May-June 1998. Results from two case studies have been compared with *in situ* measurements from the University of Washington CV-580 aircraft.

The new retrieval technique uses only a combination of spectral bands for which the snow/ice surface albedo is relatively small, and eliminates the use of visible and other bands for which the surface reflectance is large. A large surface reflectance is problematic for two reasons. First, as demonstrated in section 2, it is not likely that the

surface reflectance can be specified to the level of accuracy needed for useful optical thickness retrievals. This applies to the spatial and temporal scales needed for global studies, as well as small-scale validation exercises near coastal or other transitional areas. Secondly, even if the surface reflectance is specified accurately, a large value diminishes the impact of the cloud contribution to the overall reflectance. This effectively reduces the sensitivity of aircraft or satellite measurements to cloud optical thickness, or conversely, the optical thickness retrieval error is increased for the same amount of measurement or cloud modeling error. However, a 1.6 μm band reflectance measurement, combined with a 2.1 μm or 3.7 μm band measurement, has sufficient information content for performing retrievals. In a sense, the 1.6 μm band is used as a surrogate for the traditional band where insignificant water droplet absorption (e.g., 0.67, 0.86 μm bands) provides a nearly independent estimate of cloud optical thickness. The advantage in this modified algorithm is that each of these longer wavelength bands has a small snow/ice surface reflectance during the time frame of the FIRE-ACE experiment (similar to dark open water). Earlier in the springtime (April), spectral sea ice albedo derived from the CAR instrument is significantly larger than in June for all bands, including the 1.6 μm band (see Fig. 3). For such a situation, algorithm advantages may not be as significant. The disadvantage with this technique is that the two cloud parameters are no longer orthogonal through much of the measurement space due to significant droplet absorption in the 1.6 μm band. An increased sensitivity to measurement error still exists compared with traditional retrievals over dark surfaces.

MAS retrievals were made for several liquid water clouds during FIRE-ACE, including the two extensive stratus case studies discussed here: a low boundary layer cloud and a midlevel supercooled cloud. In both cases, retrievals are in close agreement with CV-580 *in situ* measurements when the 1.6–2.1 μm MAS band combination is used. However, when using the 3.7 μm band, effective radius retrievals are found to be 3-5 μm larger than expected from cloud profile measurements. The source of this discrepancy is not immediately obvious. An overall impression is that results for the FIRE-ACE clouds appear very similar to previous retrievals on warm marine boundary layer stratocumulus. Future efforts will use the algorithm to derive retrieval statistics from all useful liquid water cloud observations during the ER-2 deployment period. The initial success of the technique has important implications for the future development of robust operational satellite cloud retrieval algorithms in polar and wintertime regions.

Acknowledgments. This work was supported in part by funding provided by the NASA Radiation Science Program, the MODIS Science Team, and the EOS Project Science Office. The authors wish to thank G. T. Arnold at NASA Goddard Space Flight Center; A. Rangno at the University of Washington; T. Uttal, J. Intrieri, and B. Orr of NOAA/ETL; M. Fitzgerald, P. Hajek, and J. Meyers at the NASA Ames Research Center and C. Moeller at the University of Wisconsin for MAS processing and calibration support. Ice station rawinsonde data was obtained from the SHEBA web site courtesy of the University of Washington Applied Physics Laboratory.

References

Albrecht, B.A., Aerosols, Cloud Microphysics, and Fractional Cloudiness, *Science, 245*, 1227-1230, 1989.

Arking, A., and J.D. Childs, Retrieval of cloud cover parameters from multispectral satellite images, *J. Climate Appl. Meteor., 24*, 322-333, 1985.

Arnold, G.T., S.C. Tsay, M.D. King, J.Y. Li, and P.F. Soulen, Airborne spectral measurements of surface-atmosphere anisotropy for Arctic sea ice and tundra, *Int. J. Remote Sens.* (submitted), 2000.

Austin, P., Y. Wang, R. Pincus, and V. Kujala, Precipitation in stratocumulus clouds: observational and modeling results, *J. Atmos. Sci., 52*, 2329-2352, 1995.

Bohren, C.F., Multiple scattering of light and some of its observable consequences, *Amer. J. Phys., 55*, 524-533, 1987.

Charlson, R.J., J.E. Lovelock, M.O. Andreae, and S.G. Warren, Oceanic Phytoplankton, Atmospheric Sulfur, Cloud Albedo and Climate, *Nature, 326*, 655-661, 1987.

Curry, J.A., and e. al., FIRE Arctic Clouds Experiment, *Bull. Amer. Meteor. Soc., in press*, 1999.

DeAbreu, R.A., D.G. Barber, K. Misurak, and E.F. LeDrew, Spectral albedo of snow-covered first-year and multi-year sea ice during spring melt, *Ann. Glaciol., 21*, 337-342, 1995.

Foot, J.S., Some observations of the optical properties of cloud. Part I: Stratocumulus., *Quart. J. Roy. Meteor. Soc., 114*, 129-144, 1988.

Gerber, H., B.G. Arends, and A.S. Ackerman, New microphysics sensor for aircraft use, *Atmos. Res., 31*, 235-252, 1994.

Grenfell, T.C., and D.K. Perovich, Spectral albedo of sea ice and incident solar irradiance in the southern Beaufort Sea, *J. Geophys. Res., 89*, 3573-3580, 1984.

Han, Q., W.B. Rossow, and A.A. Lacis, Near-global survey of effective droplet radii in liquid water clouds using ISCCP data, *J. Climate, 7*, 465-497, 1994.

King, M.D., W.P. Menzel, P.S. Grant, J.S. Myers, G.T. Arnold, S.E. Platnick, L.E. Gumley, S.C. Tsay, C.C. Moeller, M. Fitzgerald, K.S. Brown, and F.G. Osterwisch, Airborne scanning spectrometer for remote sensing of cloud, aerosol, water vapor, and surface properties, *J. Atmos. Oceanic Tech., 13*, 777-794, 1996.

Nakajima, T., and M.D. King, Determination of the optical thickness and effective particle radius of clouds from reflected solar radiation measurements. I. Theory, *J. Atmos. Sci., 47*, 1878-1893, 1990.

Nakajima, T., M.D. King, J.D. Spinhirne, and L.F. Radke, Determination of the optical thickness and effective particle radius of clouds from reflected solar radiation

measurements. II. Marine stratocumulus observations, *J. Atmos. Sci.*, *48*, 728-750, 1991.

Ou, S.C., K.N. Liou, Y. Takano, N.X. Rao, Q. Fu, A.J. Heymsfield, L.M. Miloshevich, B. Baum, and S.A. Kinne, Remote sounding of cirrus cloud optical depths and ice crystal sizes from AVHRR data: Verification using FIRE II IFO measurements, *J. Atmos. Sci.*, *52*, 4143-4158, 1995.

Pincus, R., and M.B. Baker, Effect of precipitation on the albedo susceptibility of clouds in the marine boundary layer, *Nature*, *372*, 250-252, 1994.

Platnick, S., Vertical photon transport in cloud remote sensing problems, *J. Geophys. Res.*, (submitted), 1999.

Platnick, S., P.A. Durkee, K. Nielsen, J.P. Taylor, S.-C. Tsay, M.D. King, R.J. Ferek, P.V. Hobbs, and J.W. Rottman, The role of background cloud microphysics in the radiative formation of ship tracks, *J. Atmos. Sci.*, *in press*, 2000.

Platnick, S., and S. Twomey, Determining the susceptibility of cloud albedo to changes in droplet concentrations with the Advanced Very High Resolution Radiometer, *J. Appl. Meteor.*, *33*, 334-347, 1994.

Platnick, S., and F.P.J. Valero, A validation of a satellite cloud retrieval during ASTEX, *J. Atmos. Sci.*, *52*, 2985-3001, 1995.

Rawlins, F., and J.S. Foot, Remotely sensed measurements of stratocumulus properties during FIRE using the C130 aircraft multi-channel radiometer, *J. Atmos. Sci.*, *47*, 2488-2503, 1990.

Slingo, A., Sensitivity of the Earth's Radiation Budget to Changes in Low Clouds, *Nature*, *343*, 49-51, 1990.

Thekaekara, M.P., Extraterrestrial solar spectrum, 3000-6100 A at 1-A intervals, *Appl. Opt.*, *13*, 518-522, 1974.

Tsay, S.C., M.D. King, G.T. Arnold, and J.Y. Li, Airborne spectral surface measurements of surface anisotropy during SCAR-B, *J. Geophy. Res.*, *103*, 31943-31953, 1988.

Twomey, S., Pollution and the planetary albedo, *Atmos. Environ.*, *8*, 1251-1256, 1974.

Twomey, S., Aerosols, clouds, and radiation, *Atmos. Environ.*, *25A*, 2435-2442, 1991.

Twomey, S., and T. Cocks, Spectral reflectance of clouds in the near-infrared: Comparison of measurements and calculations, *J. Meteor. Soc. Japan*, *60*, 583-592, 1982.

Wielicki, B.A., R.D. Cess, M.D. King, D.A. Randall, and E.F. Harrison, Mission to Planet Earth - Role of Clouds and Radiation in Climate, *Bull. Amer. Meteor. Soc.*, *76*, 2125-2153, 1995.

Young, D.F., P. Minnis, D. Baumgardner, and H. Gerber, Comparison of in situ and satellite-derived cloud properties during SUCCESS, *Geophys. Res. Lett.*, *25*, 1125-1128, 1998.

List of Figures

Fig. 1. Cloud retrieval solution space showing contours of constant optical thickness (τ_c) and droplet effective radius (r_e) as a function of 0.67 and 2.1 μm band reflectances. A point specified by measurements in the two spectral bands gives the solution. Two different surface albedos in the visible are considered: (a) Lambertian reflectance of 0.06 corresponding to open water, and (b) reflectance of 0.50 corresponding to sea ice. Calculations are for μ_0=0.55, μ=0.85, and an azimuthal average.

Fig. 2. Same as Fig. 1, but retrieval solution space as a function of (a) 1.6 and 2.1 μm band reflectances, and (b) 1.6 and 3.7 μm band reflectances. Surface albedos in both spectral bands correspond to sea ice measurements as described in the text.

Fig. 3. Sea ice and snow albedo derived from CAR measurements in the vicinity of Barrow, AK during April 1992 (LEADEX, open triangles) and June 1995 (ARMCAS, closed symbols). Also shown are selected MAS sea ice bidirectional reflectance measurements on 29 May 1998 during FIRE-ACE.

Fig. 4. MAS 0.67 μm band geolocated images of the Barrow, AK area on two clear-sky days: 29 May 1998 (top image) and 2 June 1998 (bottom). Complete melting of snow/ice on the tundra occurred during the four days between images, along with significant movement of offshore ice.

Fig. 5. MAS 0.67 μm band geolocated image of an extensive lowlevel stratus deck in the Barrow, AK area on 6 June 1998 (top image) where differing surface reflectances are clearly seen through the cloud. Corresponding 1.6 μm image (bottom) with small surface reflectances for snow/ice and wet tundra indicates a relatively uniform cloud across the land-ocean boundary.

Fig. 6a. Cloud optical thickness retrievals for the 6 June 1998 lowlevel stratus deck of Fig. 5 using MAS 1.6 and 2.1 μm bands. Optical thickness is seen to be continuous across the land-ocean boundary while a dramatic decrease is seen across the cloud boundary to the north. The notation *N.R.* on the color bar refers to no retrieval.

Fig. 6b. Same as in Fig. 6a, but retrieval of cloud droplet effective radius.

Fig. 6c. Same as in Fig. 6a, but retrieval of cloud liquid water path.

Fig. 7a. MAS visible band image (far left) showing a midlevel liquid water stratus deck (cloud top heights at approximately 3.3. km throughout the three distinct cloud regions) on 3 June 1998 in the vicinity of the SHEBA ice station. Corresponding retrievals using the 1.6 and 2.1 μm MAS bands are shown to the right. The approximate location of the cloud region sampled by the *in situ* probes about 10 minutes after the overpass is also indicated.

Fig. 7b. Same as in Fig. 7a, but for retrievals using the 1.6 and 3.7 μm MAS bands.

Table 1a. MAS retrieval summary (derived from two flight tracks) and comparison with University of Washington CV-580 in situ measurements, 3 June 1998.

Parameter	MAS retrievals* (statistics)	UW CV-580 (derived from profile measurements)
τ	14.4	10.7-13.9[1]
σ_τ	1.5	
r_e (μm)	8.3	8.1[2]
σ_{re}	0.6	
LWP ($g\,m^{-2}$)	80	45-56[3]
σ_{LWP}	10	

Table 1b. MAS retrieval summary and comparison with University of Washington CV-580 in situ measurements, on 6 June 1998.

Parameter	MAS retrievals* (statistics)	UW CV-580 (derived from profile measurements)
τ	10.4	8.6[1]
σ_τ	1.7	
r_e (μm)	9.3	9.0[2]
σ_{re}	1.1	
LWP ($g\,m^{-2}$)	64	60[3]
σ_{LWP}	10	

**retrievals using 1.6μm and 2.1μm MAS bands; [1] Integrating nephelometer, Gerber Scientific, Inc.; [2] FSSP-100 (expected retrieval range based on adiabatic vertical profile); [3] PVM-100A.*

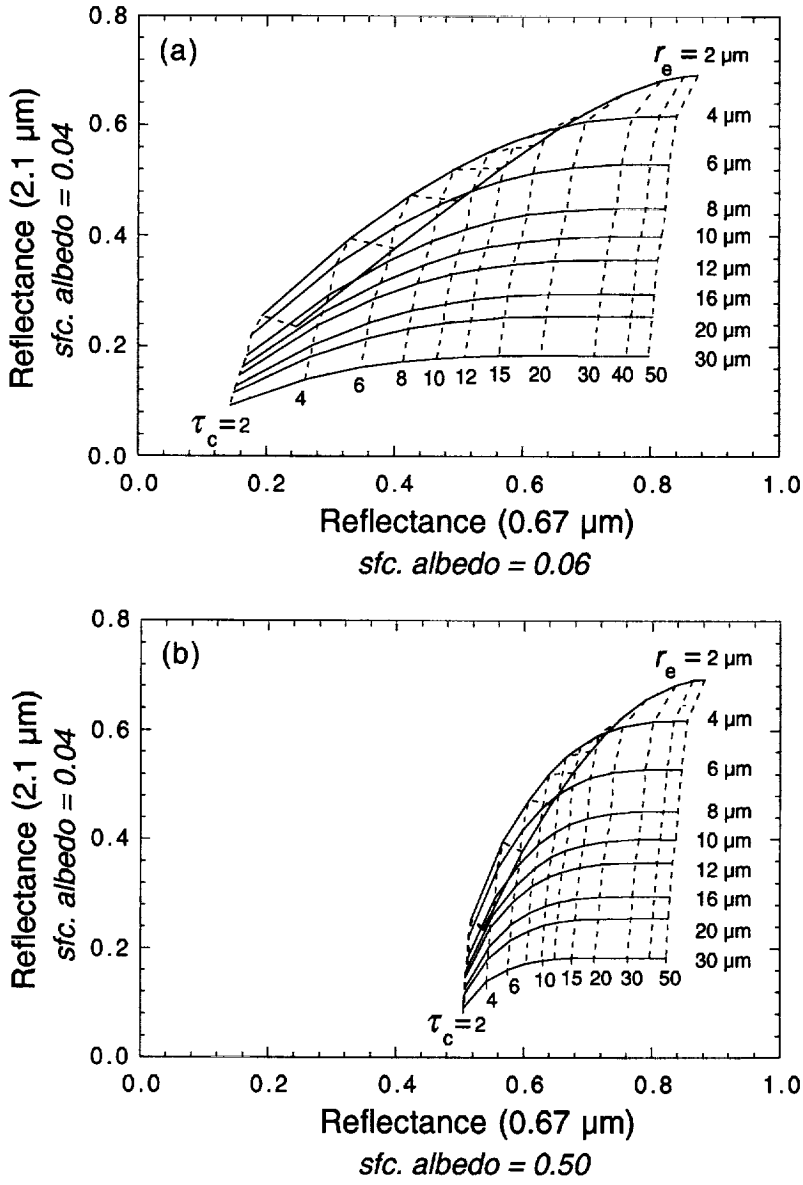

Figure 1. Cloud retrieval solution space showing contours of constant optical thickness (τ_c) and droplet effective radius (r_e) as a function of 0.67 and 2.1 μm band reflectances. A point specified by measurements in the two spectral bands gives the solution. Two different surface albedos in the visible are considered: (a) Lambertian reflectance of 0.06 corresponding to open water, and (b) reflectance of 0.50 corresponding to sea ice. Calculations are for μ_0=0.55, μ=0.85, and an azimuthal average.

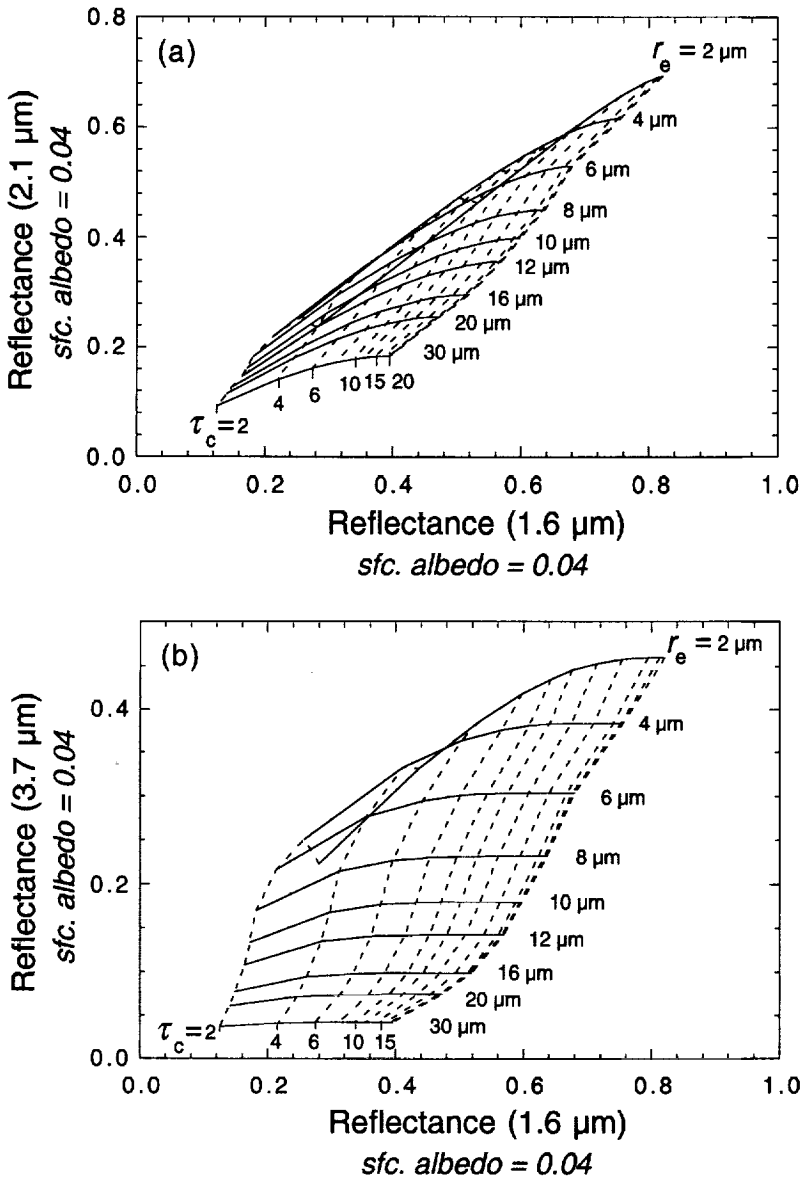

Figure 2. Same as Fig. 1, but retrieval solution space as a function of (a) 1.6 and 2.1μm band reflectances, and (b) 1.6 and 3.7μm band reflectances. Surface albedos in both spectral bands correspond to sea ice measurements as described in the text.

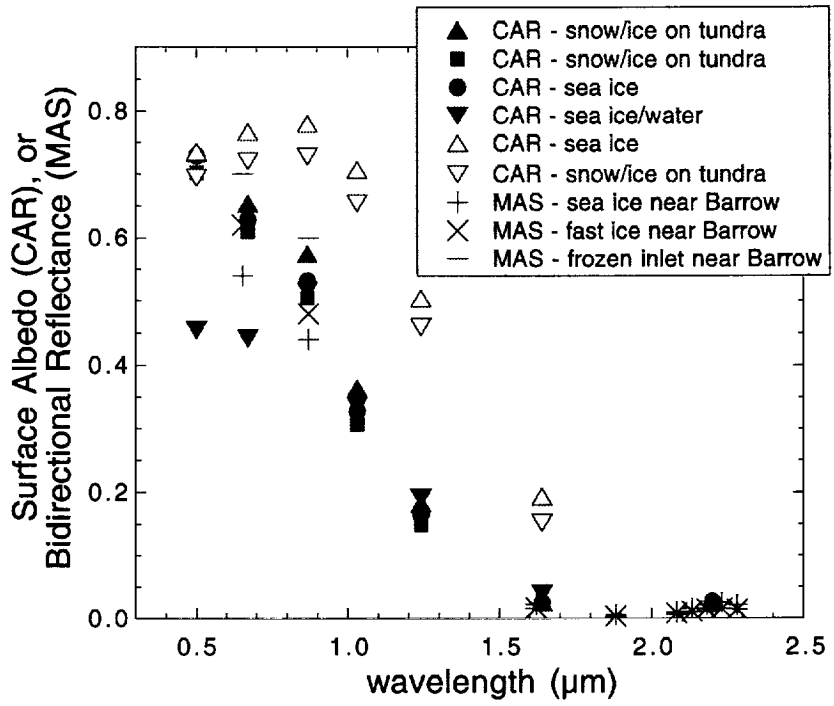

Figure 3. Sea ice and snow albedo derived from CAR measurements in the vicinity of Barrow, AK during April 1992 (LEADEX, open triangles) and June 1995 (ARMCAS, closed symbols). Also shown are selected MAS sea ice bidirectional reflectance measurements on 29 May 1998 during FIRE-ACE.

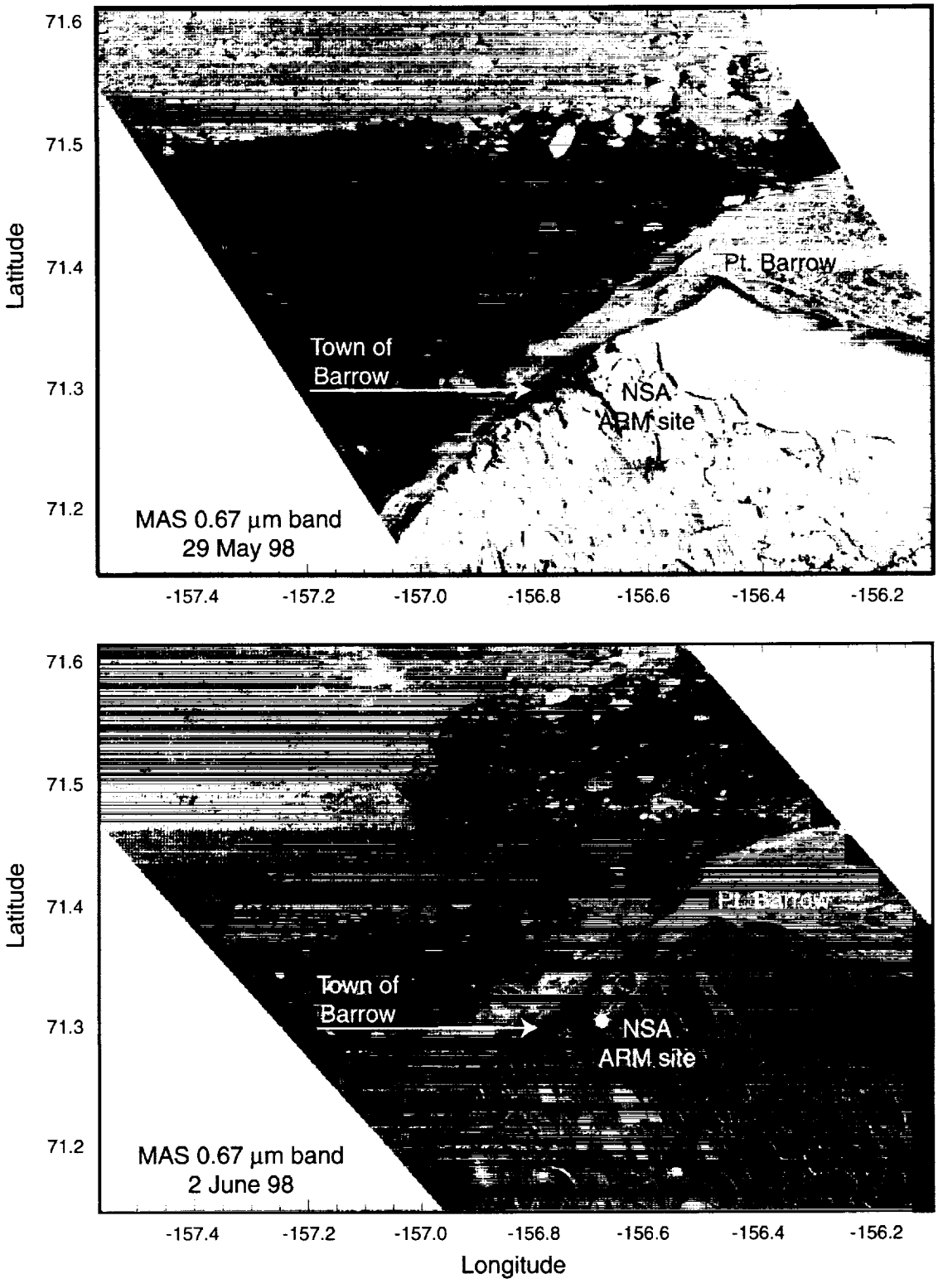

Figure 4. MAS 0.67 µm band geolocated images of the Barrow, AK area on two clear-sky days: 29 May 1998 (top image) and 2 June 1998 (bottom). Complete melting of snow/ice on the tundra occurred during the four days between images, along with significant movement of offshore ice.

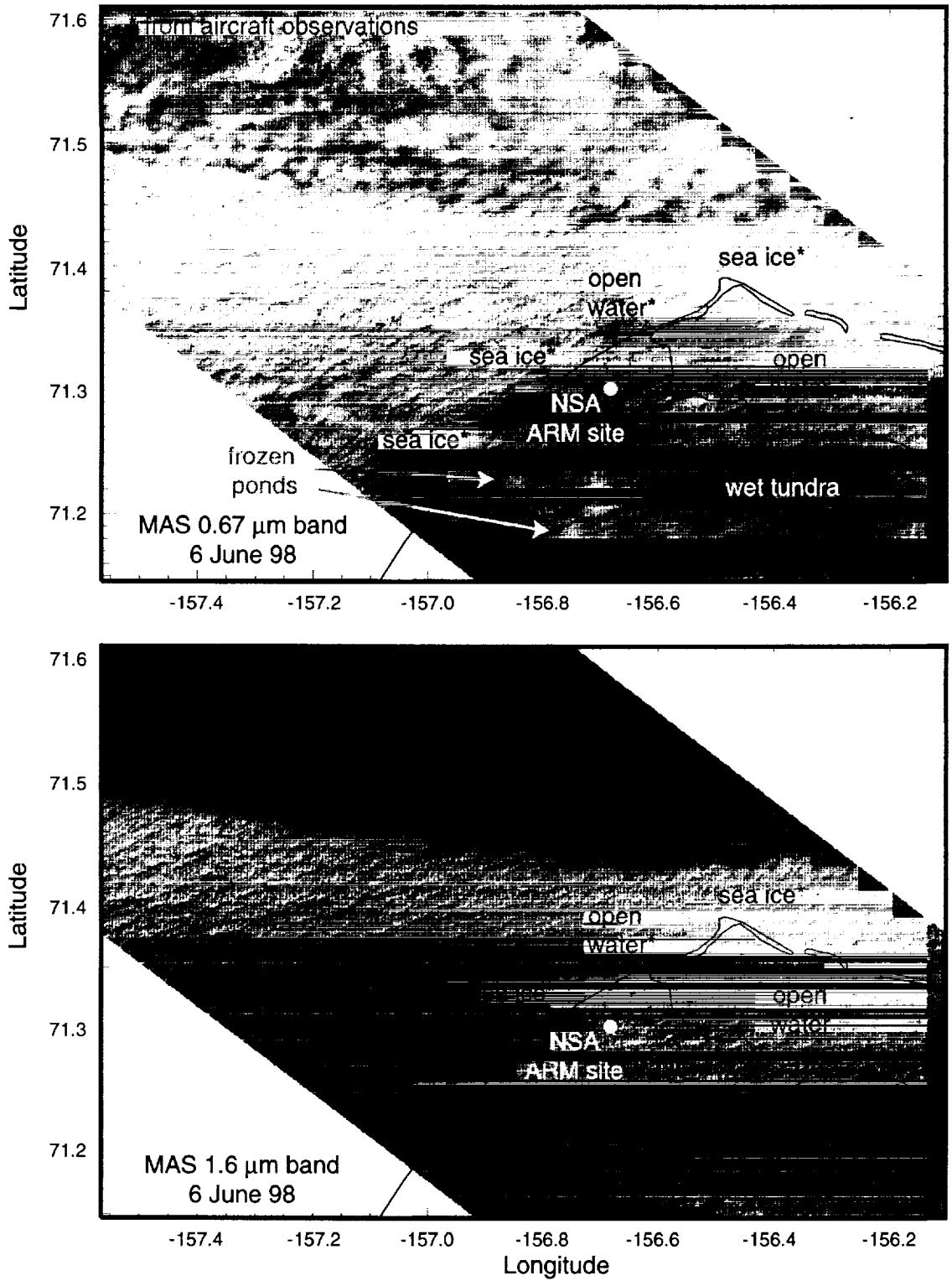

Figure 5. MAS 0.67 µm band geolocated image of an extensive low level stratus deck in the Barrow, AK area on 6 June 1998 (top image) where differing surface reflectances are clearly seen through the cloud. Corresponding 1.6 µm image (bottom) with small surface reflectances for snow/ice and wet tundra indicates a relatively uniform cloud across the land-ocean boundary.

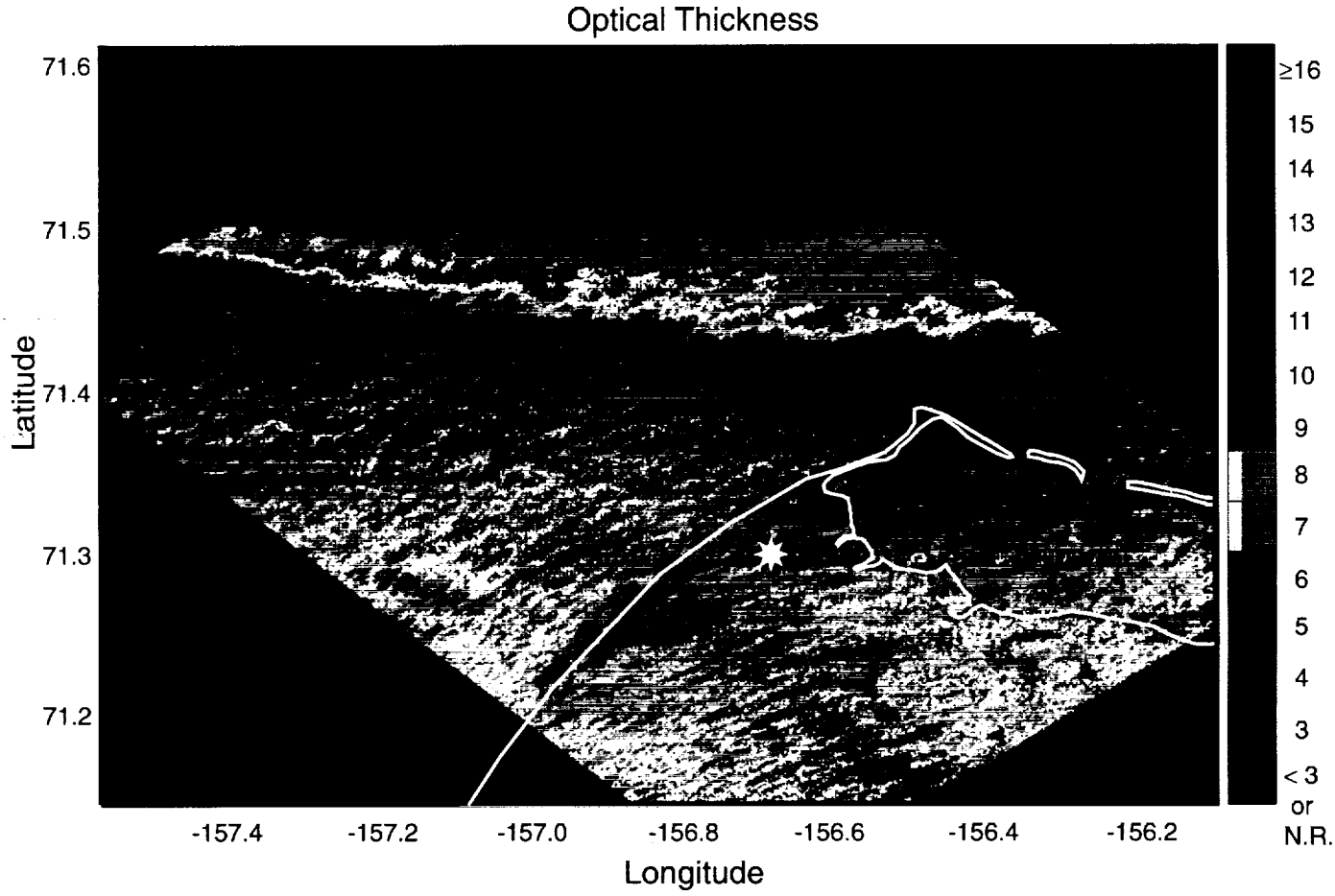

Figure 6a. Cloud optical thickness retrievals for the 6 June 1998 low level stratus deck of Fig. 5 using MAS 1.6 and 2.1 μm bands. Optical thickness is seen to be continuous across the land-ocean boundary while a dramatic decrease is seen across the cloud boundary to the north. The notation *N.R.* on the color bar refers to no retrieval.

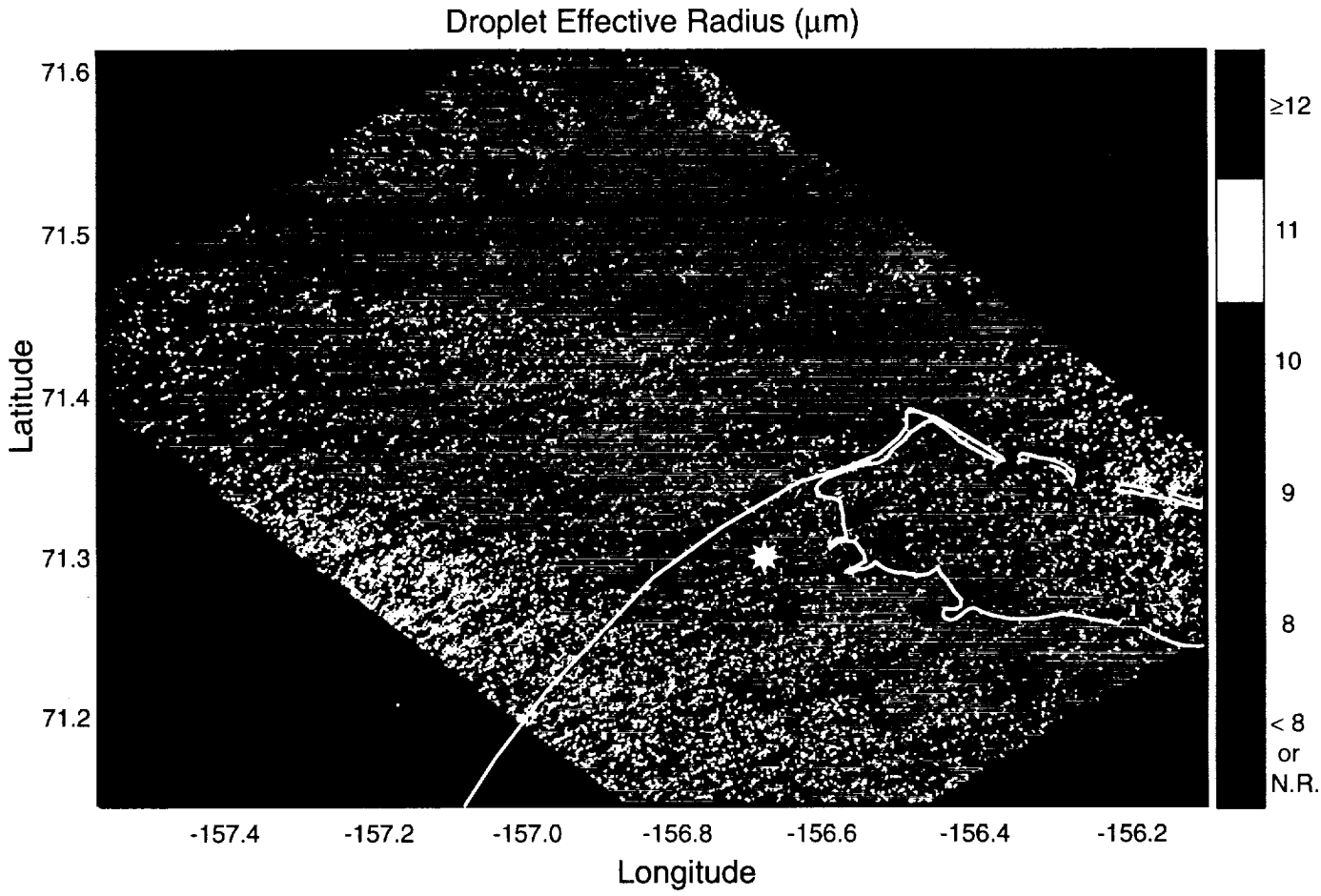

Figure 6b. Same as in Fig. 6a, but retrieval of cloud droplet effective radius.

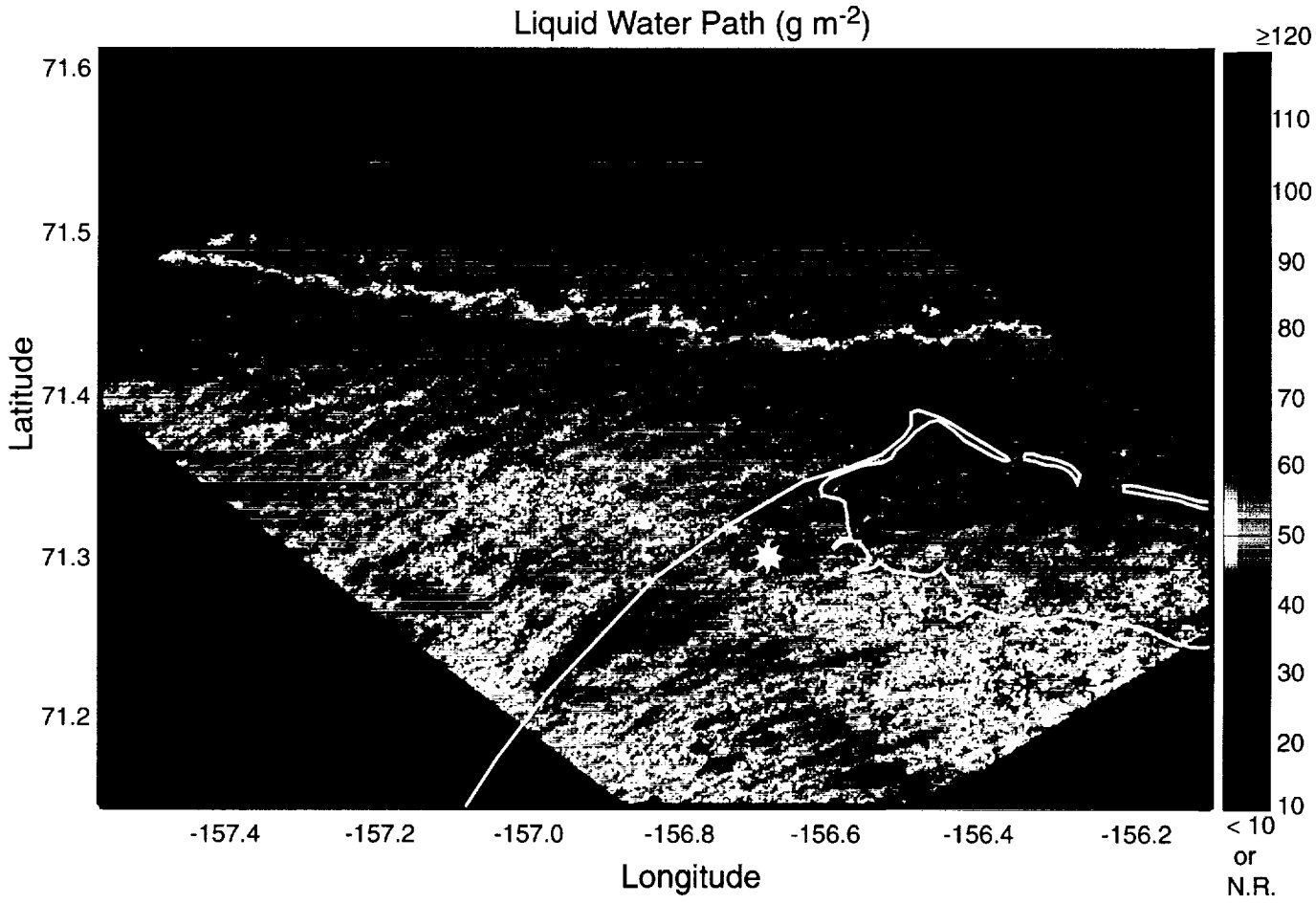

Figure 6c. Same as in Fig. 6a, but retrieval of cloud liquid water path.

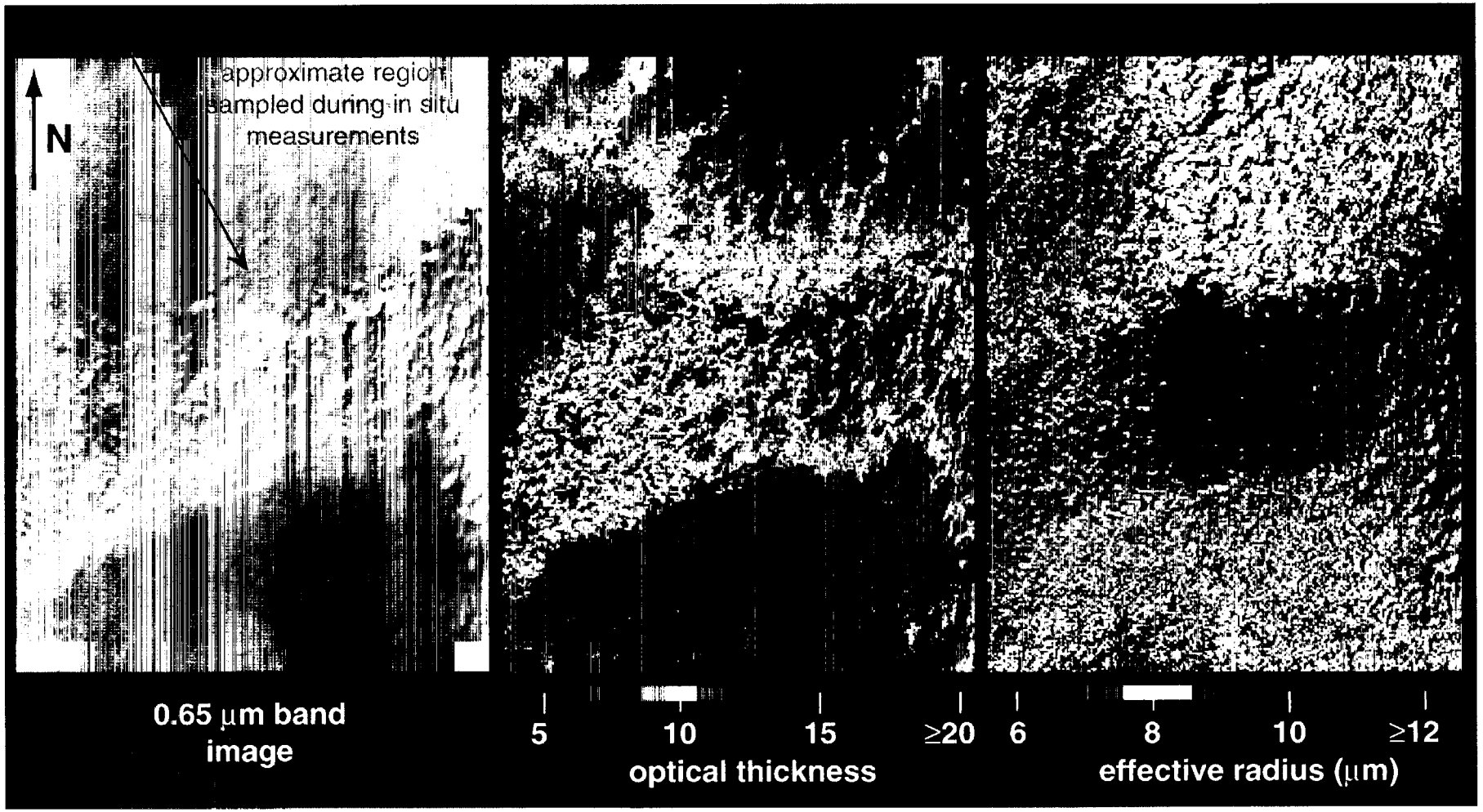

Figure 7a. MAS visible band image (far left) showing a mid level liquid water stratus deck (cloud top heights approximately 3.3 km throughout the three distinct cloud regions) on 3 June 1998 in the vicinity of the SHEBA ice station. Corresponding retrievals using the 1.6 and 2.1 μm MAS bands are shown to the right. The approximate location of the cloud region sampled by the in situ probes about 10 minutes after the overpass is also indicated.

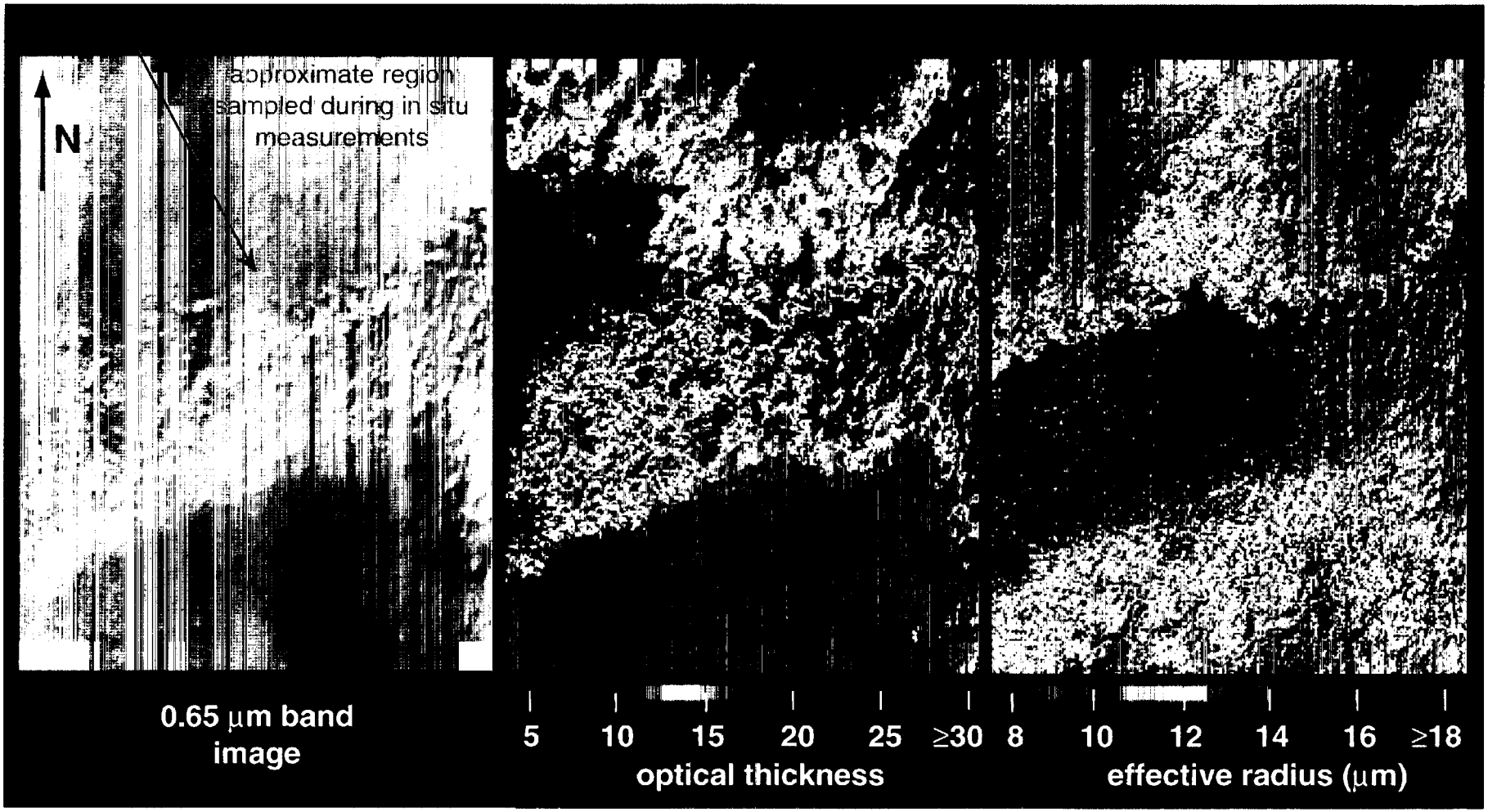

Figure 7b. Same as Fig. 7a, but for retrievals using the 1.6 and 3.7 μm MAS bands.